Composite Structures 180 (2017) 221–233

Contents lists available at ScienceDirect

Composite Structures

journal homepage: www.elsevier.com/locate/compstruct

# Dynamic stationary crack analysis of isotropic solids and anisotropic composites by enhanced local enriched consecutive-interpolation elements

Zuoyi Kang [a], Tinh Quoc Bui [a,*], Du Dinh Nguyen [b], Sohichi Hirose [a]

[a] Department of Civil and Environmental Engineering, Tokyo Institute of Technology, 2-12-1-W8-22, Ookayama, Meguro-ku, Tokyo 152-8552, Japan
[b] Department of Civil Engineering, Lac Hong University, Dong Nai Province, Viet Nam

ARTICLE INFO

*Article history:*
Received 23 April 2017
Revised 13 July 2017
Accepted 3 August 2017
Available online 4 August 2017

*Keywords:*
Fracture
Dynamic stress intensity factors
Consecutive-interpolation procedure
XFEM
Composite materials
FEM

ABSTRACT

The recently developed local enriched consecutive-interpolation 4-node quadrilateral element (XCQ4) is extended to study transient dynamic stress intensity factors (DSIFs) for isotropic solids and anisotropic composite materials containing stationary cracks. The XCQ4 involves both nodal values and averaged nodal gradients as interpolation conditions to smooth the distribution of unknown variables. The possible physical properties of enriched nodes in consecutive-interpolation procedure (CIP) would be thought as non-locality feature, which could improve the accuracy of results and eliminate the non-smooth stresses among inter-elements. In XCQ4, the crack is determined by level set function and enriched by Heaviside and crack-tip enrichment functions with special anisotropic enriched crack-tip functions. Time-dependent discrete equations for dynamic cracks are solved by Newmark time integration scheme at each time step without considering the effects of velocity-based global damping matrix. The proposed method is verified through a series of numerical examples of transient fracture in both isotropic and anisotropic materials. Numerical DSIFs are compared with reference solutions available in literature. The behavior of dynamic response is explored in specimens with complex configuration under step and sine loads.



## 1. Introduction

Composite materials featuring the light weight, high strength etc. have been widely applied to product design and engineering structure in the past decades. The investigation with respect to material property inside anisotropic solids has arisen as one important research topic. Dynamic fracture issues of composite materials always occur in the fields of aviation, infrastructure, automotive and so on, which requires targeted study to clarify the complex mechanism of dynamic fracture behavior in the anisotropic materials. On account of the increase of material constants, anisotropic fundamental solutions become more complicated to be determined than those of isotropic media [1]. Fracture mechanism of composite material and elastodynamic behavior in an anisotropic medium have been studied, e.g., see [2–6]. Based on the analytical works, the stress and displacement formulation around linear crack in anisotropic solids can be obtained.

Due to the restriction of analytical methods, especially for dynamic problems, numerical methods become important and preferable to simulate the fracture behavior in composite materials. Based on the implementation of time-harmonic, Laplace-domain or time-domain BEM [7–9] for dynamic crack analysis, the dynamic fundamental solutions in anisotropic materials can be gained. Nguyen et al. [10] investigated the transient dynamic stress intensity factors (DSIFs) in orthotropic material using an extended meshfree radial point interpolation method (X-RPIM), which further enhances the application of meshfree methods [11,12] by combination of a ramp function to describe crack tip. The edge-based strain smoothing technique [13] using a special singular element or the extended isogeometric analysis in terms of local partition of unity method [14,15] has also been introduced and applied to deal with fracture problems in multiphase materials. Other approaches related to anisotropic shell theory [16,17], numerical implementation [18,19] are devoted to explore the influence of anisotropic mechanical properties on shear or buckling damage of plates.

Finite element method (FEM) [20] is well known, as a powerful technique, and has been used for solving many engineering

* Corresponding author.
*E-mail address:* bui.t.aa@m.titech.ac.jp (T.Q. Bui).

http://dx.doi.org/10.1016/j.compstruct.2017.08.021
0263-8223/

problems. It is capable of providing robust solutions for non-linear, plastic, dynamic problems and can treat arbitrary boundary conditions and complicated configuration of various cases. Shetty et al. [21] provided an overall literature review on machining of composites which focuses on simulation methods containing discrete element method and FEM. For numerical fracture solutions, the extended finite element method (XFEM) (e.g., see [22–25] and references therein) is more advantageous than the FEM, which requires crack modelling align with finite element mesh and remeshing procedure in crack propagation problem [22]. Mohammadi [26,27] comprehensively demonstrates the application of XFEM for fracture analysis of structures and composite materials. Furthermore, the elasticity solution for isotropic bi-material interface, XFEM modelling for a contact problem and dynamic orthotropic LEFM, etc., have also been involved. Asadpoure et al. [28,29] and Hattori et al. [30] explored fracture properties of orthotropic models and proposed a new set of enrichment functions for crack modelling in orthotropic solids, and using the interaction integral for calculating SIFs under the framework of XFEM.

Accurate estimation of DSIFs is essential and imperative to analyze dynamic fracture mechanism of composite materials. Transient dynamic problems for stationary and moving crack were conducted by, for instance, [13,31–33]. Song [34] evaluated DSIFs by incorporating dynamic effects into homogeneous and non-homogeneous material and found that M-integral is superior to the displacement correlation technique (DCT) compared with J-integral Albuquerque et al. [35] who computed DSIFs based on the crack opening displacements using a dual boundary element method. The elastodynamic response induced by an in-plane shear load in orthotropic material was investigated by Rubio-Gonzalez et al. [36].

Recently, Bui et al. [37,38] proposed a new 4-node quadrilateral element with continuous nodal stress using the consecutive-interpolation procedure (CQ4) for stress and transient analysis of 2D elastic and piezoelectric solids. Kang et al. [25,39] enhanced the CQ4 by enrichments, named as XCQ4, for linear fracture and crack propagation problems [31,32,38]. The advantage of the proposed method over the conventional XFEM is higher accuracy of the gradients of trial solutions causing more accurate calculation of interaction integral. In addition, the proposed approach sustains a total number of the degrees of freedom (DOFs) as constant, implying that no additional DOFs are needed [37].

The purpose of this study is to enhance our XCQ4 framework to analyze the dynamic fracture response in isotropic and anisotropic materials. The prediction of DSIFs time history for both single and mixed-mode fracture problems is presented and analyzed. The Heaviside function and asymptotic crack tip branch functions are integrated as enrichment to capture singular behavior near crack tips for isotropic material. For anisotropic or orthotropic material, versatile crack tip enrichment functions spanning all possible displacement states are adopted. In addition, the time-dependent discrete equations are solved using Newmark time integration without considering damping matrix. The numerical values of DSIFs are extracted according to interaction integral taking into account inertial effect. The DSIFs derived from XCQ4 for isotropic and anisotropic solids are verified with respect to reference solutions reported in literature.

This study is divided into seven sections. Firstly fracture mechanics for 2D orthotropic material is briefly presented in Section 2. Subsequently, the displacement approximation by XCQ4 method and the characteristic of CQ4 shape function are presented in Section 3. Section 4 provides the procedures of calculating DSIFs in isotropic and orthotropic materials and the visualization of support domain for $J$-domain in terms of the XCQ4. In Section 5, the corresponding weak form of the governing equation and time discretization are introduced, respectively. Besides, the Newmark time integration theme is involved. Particularly, some representative benchmark dynamic problems of cracked isotropic and orthotropic solids are solved by XCQ4. The computed DSIFs are presented and discussed in Section 6. Some major conclusions drawn from this work are given in Section 7.

## 2. Fracture characteristics of two-dimensional orthotropic material

Consider a 2-D cracked anisotropic solid subjected to traction **t** as shown in Fig. 1. Global coordinate system $(X, Y)$, local coordinate $(x, y)$ and local crack tip polar coordinate system $(r, \theta)$ are defined, respectively. The relationship between stress and strain for linear elastic material can be written as

$$\varepsilon_{ij} = s_{ijpq}\sigma_{pq} \quad (i,j,p,q = 1,2,3) \tag{1}$$

where $\varepsilon_{ij}$, $\sigma_{pq}$ and $s_{ijpq}$ are components of linear strain tensor, stress tensor and fourth-order compliance tensor respectively. For simple implementation, the compact form of Eq. (1) can be rewritten as

$$\varepsilon_{\alpha} = a_{\alpha\beta}\sigma_{\beta} \quad (\alpha,\beta = 1,2,3) \tag{2}$$

Upon considering equilibrium and compatibility conditions, a fourth-order characteristic equation can be obtained as

$$a_{11}\mu^4 - 2a_{16}\mu^3 + (2a_{12} + a_{66})\mu^2 - 2a_{26}\mu + a_{22} = 0 \tag{3}$$

The roots of Eq. (3) are always in conjugate pairs as $(\mu_1, \overline{\mu_1})$, and $(\mu_2, \overline{\mu_2})$. The displacement and stress fields in the vicinity of the crack tip have been elaborated by Asadpoure et al. [28,29]. Based on the analytical functions and complex variables $(z_k = x + \mu_k y_k k = 1,2)$, the corresponding expression of displacements and stresses for pure mode I is given by.

$$u_1 = K_I \times \sqrt{\frac{2r}{\pi}}\mathrm{Re}\left[\frac{1}{\mu_1 - \mu_2}\left\{\mu_1 p_2\sqrt{\cos\theta + \mu_2\sin\theta} - \mu_2 p_1\sqrt{\cos\theta + \mu_1\sin\theta}\right\}\right] \tag{4-1}$$

$$u_2 = K_I \times \sqrt{\frac{2r}{\pi}}\mathrm{Re}\left[\frac{1}{\mu_1 - \mu_2}\left\{\mu_1 q_2\sqrt{\cos\theta + \mu_2\sin\theta} - \mu_2 q_1\sqrt{\cos\theta + \mu_1\sin\theta}\right\}\right] \tag{4-2}$$

$$\sigma_{11} = \frac{K_I}{\sqrt{2\pi r}}\mathrm{Re}\left[\frac{\mu_1\mu_2}{\mu_1 - \mu_2}\left\{\frac{\mu_2}{\sqrt{\cos\theta + \mu_2\sin\theta}} - \frac{\mu_1}{\sqrt{\cos\theta + \mu_1\sin\theta}}\right\}\right] \tag{4-3}$$

$$\sigma_{22} = \frac{K_I}{\sqrt{2\pi r}}\mathrm{Re}\left[\frac{1}{\mu_1 - \mu_2}\left\{\frac{\mu_1}{\sqrt{\cos\theta + \mu_2\sin\theta}} - \frac{\mu_2}{\sqrt{\cos\theta + \mu_1\sin\theta}}\right\}\right] \tag{4-4}$$

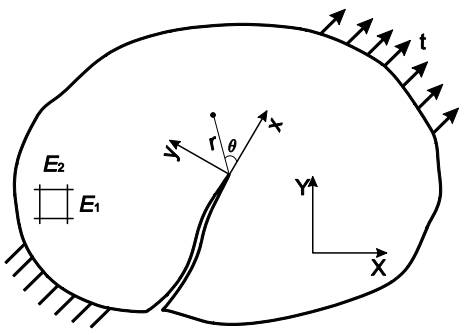


**Fig. 1.** Boundary condition for an arbitrary cracked orthotropic domain.

$$\sigma_{12}=\frac{K_I}{\sqrt{2\pi r}}\mathrm{Re}\left[\frac{\mu_1\mu_2}{\mu_1-\mu_2}\left\{\frac{1}{\sqrt{\cos\theta+\mu_1\sin\theta}}-\frac{1}{\sqrt{\cos\theta+\mu_2\sin\theta}}\right\}\right] \tag{4-5}$$

In the same manner, the displacements and stresses for pure mode II are

$$u_1=K_{II}\times\sqrt{\frac{2r}{\pi}}\mathrm{Re}\left[\frac{1}{\mu_1-\mu_2}\left\{p_2\sqrt{\cos\theta+\mu_2\sin\theta}-p_1\sqrt{\cos\theta+\mu_1\sin\theta}\right\}\right] \tag{5-1}$$

$$u_2=K_{II}\times\sqrt{\frac{2r}{\pi}}\mathrm{Re}\left[\frac{1}{\mu_1-\mu_2}\left\{q_2\sqrt{\cos\theta+\mu_2\sin\theta}-q_1\sqrt{\cos\theta+\mu_1\sin\theta}\right\}\right] \tag{5-2}$$

$$\sigma_{11}=\frac{K_{II}}{\sqrt{2\pi r}}\mathrm{Re}\left[\frac{1}{\mu_1-\mu_2}\left\{\frac{\mu_2^2}{\sqrt{\cos\theta+\mu_2\sin\theta}}-\frac{\mu_1^2}{\sqrt{\cos\theta+\mu_1\sin\theta}}\right\}\right] \tag{5-3}$$

$$\sigma_{22}=\frac{K_{II}}{\sqrt{2\pi r}}\mathrm{Re}\left[\frac{1}{\mu_1-\mu_2}\left\{\frac{1}{\sqrt{\cos\theta+\mu_2\sin\theta}}-\frac{1}{\sqrt{\cos\theta+\mu_1\sin\theta}}\right\}\right] \tag{5-4}$$

$$\sigma_{12}=\frac{K_{II}}{\sqrt{2\pi r}}\mathrm{Re}\left[\frac{1}{\mu_1-\mu_2}\left\{\frac{\mu_1}{\sqrt{\cos\theta+\mu_1\sin\theta}}-\frac{\mu_2}{\sqrt{\cos\theta+\mu_2\sin\theta}}\right\}\right] \tag{5-5}$$

where Re represents the real part of the value and $K_I$ and $K_{II}$ are stress intensity factors for mode I and mode II, respectively. $p_k$ and $q_k$ can be calculated by

$$p_k=a_{11}\mu_k^2+a_{12}-a_{16}\mu_k \tag{6}$$

$$q_k=a_{12}\mu_k+a_{22}/\mu_k-a_{26} \tag{7}$$

## 3. The extended consecutive-interpolation method

In terms of the partition of unity theory, the XFEM (see [22–27] and references therein) is an effective way to simulate discontinuity as one local enriched numerical approach. In traditional FEM, the crack should be modelled with conformation to mesh boundary and mesh refinement is required adjacent crack tips. Furthermore, remeshing procedure is imperative for crack evolution simulations. The XFEM generally can be used to alleviate such cumbersome drawbacks in crack modeling. Upon the basis of the XFEM, we develop the XCQ4 approach to obtain more accurate numerical solutions in static SIFs and quasi-static crack propagation problems, which have been investigated by Kang et al. [25,39]. In this work, the XCQ4 is further extended to study transient dynamic fracture analysis of isotropic solids and anisotropic composite materials.

### 3.1. Approximations for cracks by XCQ4

The XCQ4 composes of standard and enriched terms with additional functions to capture discontinuity and singularity. Assume one particular node of $\mathbf{x}_i$, the XCQ4 approximation of the displacements for cracks can be written as follows:

$$\mathbf{u}^h(\mathbf{x})=\sum_{i\in W_s}\tilde{N}_i(\mathbf{x})\mathbf{u}_i+\sum_{j\in W_c}\tilde{N}_j(\mathbf{x})[H(\mathbf{x})-H(\mathbf{x}_j)]\mathbf{a}_j+\sum_{k\in W_t}\tilde{N}_k(\mathbf{x})\sum_{\alpha=1}^{4}[F^\alpha(\mathbf{x})-F^\alpha(\mathbf{x}_k)]\mathbf{b}_k^\alpha \tag{8}$$

where $\tilde{N}_i(\mathbf{x})$ denotes CQ4 shape function for node $i$ that contains high order polynomials. $W_s$, $W_c$ and $W_t$ are the sets of standard nodes, Heaviside enriched nodes and crack tip enriched nodes respectively. $\mathbf{u}_i$ is the nodal displacement vector at node $i$. $\mathbf{a}_j$ and $\mathbf{b}_k^\alpha$ signify the nodal additional DOFs associated with Heaviside and asymptotic enrichment functions, respectively. $H(\mathbf{x})$ is the modified discontinuous enrichment function:

$$H(\mathbf{x})=\begin{cases}+1 & \phi(\mathbf{x})\geqslant 0\\ -1 & \phi(\mathbf{x})<0\end{cases} \tag{9}$$

where $\phi(\mathbf{x})$ is the signed distance function normal to a crack face. It should be remarked that the influence of shifted enrichment technique on the blending element is positive as stated in Sharma et al. [40], thus the blending element is not treated specially in this work.

To compute the effect of discontinuity on the stress and displacement fields in the vicinity of crack tip, the representation of crack-tip functions for orthotropic composites should consider all displacement fields given in Eqs. (4-1), (4-2), (5-1) and (5-2). Thus, the crack-tip functions for orthotropic solid can be obtained with similar form of those reported in [10,28,29]:

$$\left[F_\alpha(\mathbf{x})|_{\alpha=1}^4\right]=\left[\sqrt{r}\cos\left(\frac{\theta_1}{2}\right)\sqrt{g_1(\theta)},\sqrt{r}\cos\left(\frac{\theta_2}{2}\right)\sqrt{g_2(\theta)},\sqrt{r}\sin\left(\frac{\theta_1}{2}\right)\sqrt{g_1(\theta)},\sqrt{r}\sin\left(\frac{\theta_2}{2}\right)\sqrt{g_2(\theta)}\right] \tag{10}$$

where $g_p(\theta)$ and $\theta_p$ $(p=1,2)$ are defined as:

$$g_p(\theta)=\sqrt{(\cos\theta+\mu_{px}\sin\theta)^2+(\mu_{py}\sin\theta)^2} \tag{11}$$

$$\theta_p=arctg\left(\frac{\mu_{py}\sin\theta}{\cos\theta+\mu_{px}\sin\theta}\right) \tag{12}$$

For isotropic materials, the standard branch functions $F_\alpha(\mathbf{x})|_{\alpha=1}^4$ [22–27] to enrich asymptotic field near crack is adopted:

$$[F_\alpha(\mathbf{x})|_{\alpha=1}^4]=\left[\sqrt{r}\sin\left(\frac{\theta}{2}\right),\sqrt{r}\cos\left(\frac{\theta}{2}\right),\sqrt{r}\sin\left(\frac{\theta}{2}\right)\sin(\theta),\sqrt{r}\cos\left(\frac{\theta}{2}\right)\sin(\theta)\right] \tag{13}$$

where $(r,\theta)$ is the polar coordinate system.

### 3.2. The CQ4 shape functions

The CQ4 shape function was proposed as a modified version of standard linear one by Bui et al. [37]. The new mechanism is made up of classic shape functions and averaged gradient terms. By estimating the performance of the CQ4 method in elastic-static problems conducted by Kang et al. [25], the reliability of the CQ4 has been proven and we would like to extend the method to solve dynamic fracture issues in orthotropic material.

Consider interested point $\mathbf{x}=(x,y)$ in a quadrilateral element shown in Fig. 2. The new developed consecutive-interpolation shape function $\tilde{N}_f$ can be written as:

$$\tilde{N}_f=\underbrace{\phi_i N_f^{[i]}+\phi_{ix}\bar{N}_{f,x}^{[i]}+\phi_{iy}\bar{N}_{f,y}^{[i]}}_{\text{node } i}+\underbrace{\phi_j N_f^{[j]}+\phi_{jx}\bar{N}_{f,x}^{[j]}+\phi_{jy}\bar{N}_{f,y}^{[j]}}_{\text{node } j}+\underbrace{\phi_k N_f^{[k]}+\phi_{kx}\bar{N}_{f,x}^{[k]}+\phi_{ky}\bar{N}_{f,y}^{[k]}}_{\text{node } k}+\underbrace{\phi_m N_f^{[m]}+\phi_{mx}\bar{N}_{f,x}^{[m]}+\phi_{my}\bar{N}_{f,y}^{[m]}}_{\text{node } m} \tag{14}$$

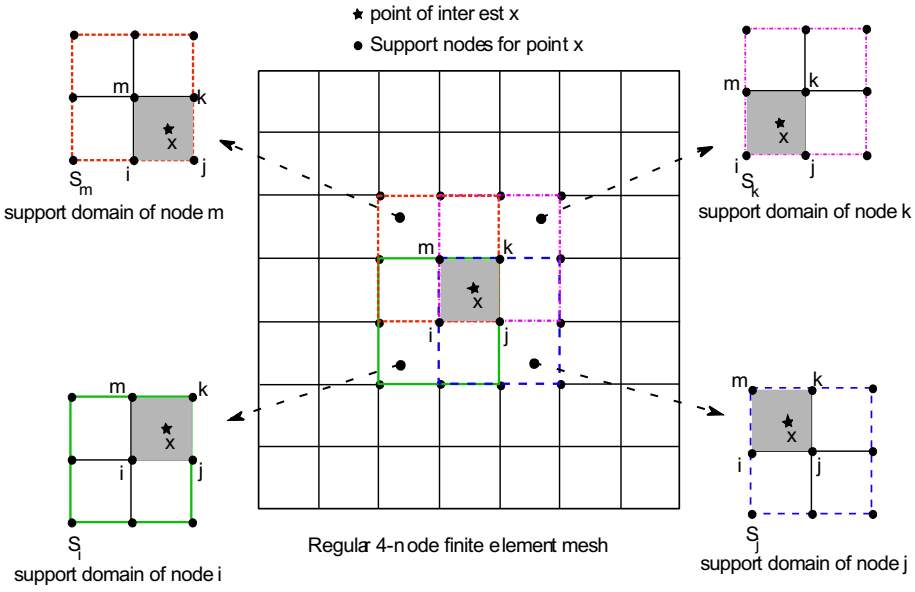


**Fig. 2.** Illustration of support domain for considered element in CQ4 algorithm [33,34,22].

where $N_f^{[i]}$ is a classic shape function and the averaged derivative terms $\bar{N}_{f,x}^{[i]}$ $\bar{N}_{f,y}^{[i]}$ can be defined as

$$\begin{aligned}\bar{N}_{f,x}^{[i]} &= \sum_{e\in S_i}(w_e N_{f,x}^{[i][e]})\\ \bar{N}_{f,y}^{[i]} &= \sum_{e\in S_i}(w_e N_{f,y}^{[i][e]})\end{aligned} \tag{15}$$

respectively. The same expression should be followed for other nodes $j,k,m$. The weight function $w_e$ and functions $\phi_i$, $\phi_{ix}$ and $\phi_{ix}$ can be written as

$$w_e = \frac{\Delta_e}{\sum_{\tilde{e}\in S_i}\Delta_{\tilde{e}}},\ \text{with } e\in S_i \tag{16}$$

$$\begin{aligned}&\phi_i(\mathbf{x}_l)=\delta_{il},\ \phi_{i,x}(\mathbf{x}_l)=0,\ \phi_{i,y}(\mathbf{x}_l)=0,\\ &\phi_{ix}(\mathbf{x}_l)=0,\ \phi_{ix,x}(\mathbf{x}_l)=\delta_{il},\ \phi_{ix,y}(\mathbf{x}_l)=0,\\ &\phi_{iy}(\mathbf{x}_l)=0,\ \phi_{iy,x}(\mathbf{x}_l)=0,\ \phi_{iy,y}(\mathbf{x}_l)=\delta_{il},\end{aligned} \tag{17}$$

where $l$ is any one of the indices $i,j,k,m$ and the other terms, i.e., $\phi_j,\phi_{jx},\phi_{jy}$, $\phi_k,\phi_{kx},\phi_{ky}$ and $\phi_m,\phi_{mx},\phi_{my}$ need follow the same way.

$$\delta_{il} = \begin{cases}1 & \text{if} \quad i=l\\ 0 & \text{if} \quad i\neq l\end{cases} \tag{18}$$

The detailed information of $\phi_l,\phi_{lx},\phi_{ly}\,(l=i,j,k,m)$ can be found in [34,35,22].

By adding the averaged gradient terms into the formulation of classic shape functions, the consecutive interpolation relationships for 1 D and 2 D cases can be illustrated in Figs. 3and 4, respectively.

*Remark #1* Due to the alleviation of the continuity caused by enriched nodes in the XCQ4 method, the modification for calculating the averaged gradient is required and related interpretation and implementation have been stated in [25,37,39].

*Remark #2* To accurately calculate the interaction integral inside enriched elements, the element partition is implemented, which will generate sub-triangles aligning to the crack surface to make the field continuous and no additional DOFs are produced. For the numerical integration order, the standard element containing no crack is treated by $2\times 2$ quadrature points in this study. For the enriched elements with a crack, high-order Gauss quadrature rules are used in each partitioned sub-triangular element to ensure the accuracy.

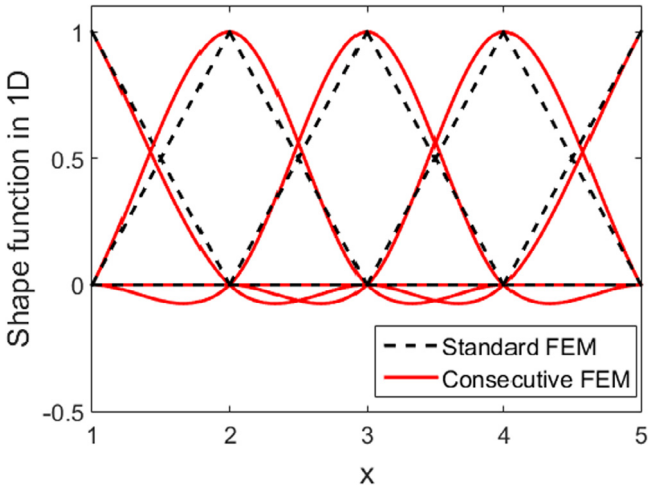


**Fig. 3.** Comparison of the standard and consecutive FEM shape functions in 1 D space.

## 4. Computation of DSIFs for isotropic and orthotropic solids

The dynamic stress intensity factors (DSIFs) are main parameters to evaluate the dynamic fracture response in the vicinity of the crack tip. The interaction integral formulated by superimposing the actual field $(\sigma_{ij}^{(1)},\varepsilon_{ij}^{(1)},u_i^{(1)})$ and auxiliary field $(\sigma_{ij}^{(2)},\varepsilon_{ij}^{(2)},u_i^{(2)})$ on the path independent $J-$integral is adopted for computation of SIFs [26,27].

By introducing a weight function q(x), the generalized $J-$integral for a closed path $C=\Gamma+C_+ +C_- +\Gamma_0$ shown in Fig. 5 can be written as [26,27]

$$\begin{aligned}J &= \lim_{\Gamma\to 0}\int_{\Gamma}(W\delta_{1j}-\sigma_{ij}u_{i,1})n_j d\Gamma\\ &= -\lim_{\Gamma\to 0}\oint_C(W\delta_{1j}-\sigma_{ij}u_{i,1})m_j q dC\end{aligned} \tag{19}$$

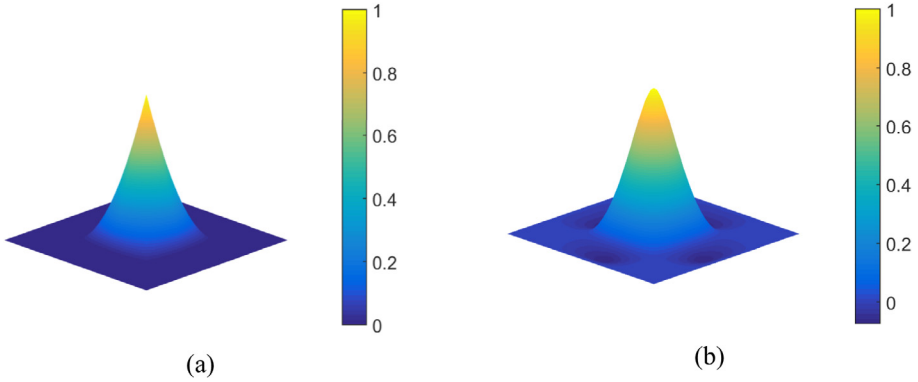


**Fig. 4.** Schematic interpretation of the standard FEM shape function (a) and the consecutive-interpolation shape function (b) in 2D space.

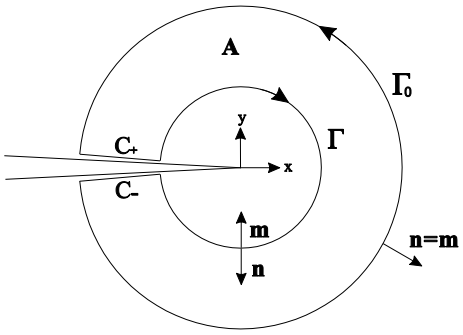


**Fig. 5.** The integral domain A for J-integral with the normal vector $m_j = -n_j \text{on}\Gamma$ and $m_j = n_j \text{on}C_+C_-\text{and}\Gamma_0$.

where $W$ is the strain energy density. $q$ is a function of smoothly changing from $q = 1$ adjacent crack tip to $q = 0$ over the exterior boundary. Additional explanation about the impact of the function $q$ on calculation of interaction integral can be found in [25].

Upon the application of the divergence theorem, the $J-$integral can be written as:

$$J = \int_A (\sigma_{ij}u_{i,1} - W\delta_{1j})q_{,j}dA + \int_A (\sigma_{ij}u_{i,1} - W\delta_{1j})_{,j}qdA \tag{20}$$

By way of some mathematical manipulation, the J-integral including material gradient and dynamic effects can be modified as

$$J^d = \int_A (\sigma_{ij}u_{i,1} - W\delta_{1j})q_{,j}dA + \int_A \left(\rho\ddot{u}_i u_{i,1} - \frac{1}{2}C_{ijkl,1}\varepsilon_{ij}\varepsilon_{kl}\right)qdA \tag{21}$$

where $C_{ijkl}$ is the elastic tensor.

The relationship between $J-$integral and SIFs $(K_I, K_{II})$ in the case of mixed mode failure can be represented as:

$$J^d = \frac{1}{E^*}(K_I^2 + K_{II}^2) \tag{22}$$

where

$$E^* = \begin{cases} E & \text{plane stress} \\ \frac{E}{1-\nu^2} & \text{plane strain} \end{cases} \tag{23}$$

By simplifying the above equations, $J-$integral can be rewritten as:

$$J^d = J^{(1)} + J^{(2)} + I^{(1,2)} \tag{24}$$

where $J^{(1)}$ and $J^{(2)}$ are $J-$integrals for actual state and auxiliary state, respectively. $I^{(1,2)}$ is the interaction integral and can be calculated by:

$$I^{(1,2)} = \int_A \left(\sigma_{ij}^{(1)}u_{i,1}^{(2)} + \sigma_{ij}^{(2)}u_{i,1}^{(1)} - \sigma_{ik}^{(2)}\varepsilon_{ik}^{(1)}\delta_{1j}\right)q_{,j}dA + \int_A \rho\ddot{u}_i^{(1)}u_{i,1}^{(2)}qdA \tag{25}$$

The relationship between the SIFs $(K_I, K_{II})$ and the interaction integral for isotropic material is expressed as:

$$I^{(1,2)} = \frac{2(K_I^{(1)}K_I^{(2)} + K_{II}^{(1)}K_{II}^{(2)})}{E^*} \tag{26}$$

$$K_I^{(1)} = (E^*/2)I^{(1,I)}; K_{II}^{(1)} = (E^*/2)I^{(1,II)} \tag{27}$$

For orthotropic material, the relationship can be defined as [29]:

$$I^{(1,2)} = 2c_{11}K_I^{(1)}K_I^{(2)} + c_{12}\left(K_I^{(1)}K_{II}^{(2)} + K_I^{(2)}K_{II}^{(1)}\right) + 2c_{22}K_{II}^{(1)}K_{II}^{(2)} \tag{28}$$

where

$$c_{11} = -\frac{a_{22}}{2}\text{Im}\left(\frac{\mu_1 + \mu_2}{\mu_1\mu_2}\right) \tag{29}$$

$$c_{12} = -\frac{a_{22}}{2}\text{Im}\left(\frac{1}{\mu_1\mu_2}\right) + \frac{a_{11}}{2}\text{Im}(\mu_1\mu_2) \tag{30}$$

$$c_{22} = -\frac{a_{11}}{2}\text{Im}(\mu_1 + \mu_2) \tag{31}$$

By setting the values of $(\text{state}1 : K_I^{(2)} = 1.0, K_{II}^{(2)} = 0.0)$ and $(\text{state}2 : K_I^{(2)} = 0.0, K_{II}^{(2)} = 1.0)$, the actual mixed –mode SIFs can be obtained through solving linear algebraic equations:

$$K_I^{(1)} = 2c_{11}I^{(1,I)} + c_{12}I^{(1,II)} \tag{32}$$

$$K_{II}^{(1)} = c_{12}I^{(1,I)} + 2c_{22}I^{(1,II)} \tag{33}$$

It is worth pointing out that the support domain for the element considered in $J$-domain in terms of the XCQ4 is larger than that used in XFEM as illustrated in Fig. 6. The reason is the implementation of the larger span formed by neighboring elements of the CIP framework [39].

## 5. Discrete equations and solutions for dynamic fracture analysis

In elastodynamic problem, the displacement $\mathbf{u}$, the velocity $\dot{\mathbf{u}}$ and the acceleration $\ddot{\mathbf{u}}$ should approximate via reconstructed function expressed in Eq. (8). The weak form for the discrete problem can be rewritten as [13]:

$$\int_\Omega \delta\mathbf{u}^T\ddot{\mathbf{u}}\rho d\Omega + \int_\Omega \nabla_s\delta\mathbf{u} : \boldsymbol{\sigma}d\Omega - \int_\Omega \delta\mathbf{u}^T\bar{\mathbf{b}}\rho d\Omega - \int_{\Gamma_t} \delta\mathbf{u}^T\bar{\mathbf{t}}\rho d\Gamma = 0 \tag{34}$$

where $\delta\mathbf{u}$ is the variational trial functions.

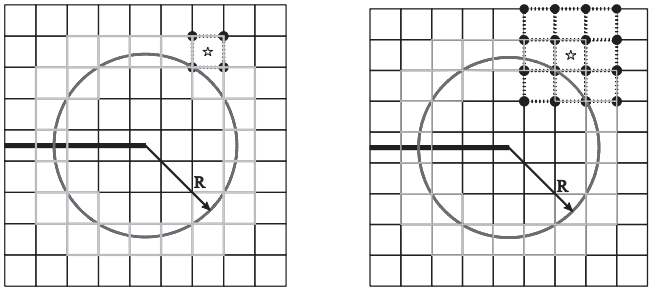


**Fig. 6.** Support domain for $J$-domain in (a) XQ4 and (b) XCQ4 [39].

By substituting the XCQ4 approximation function of Eq. (8) into the weak form Eq. (34), the discrete form can be gained as follows:

$$\mathbf{M}\ddot{\mathbf{u}} + \mathbf{K}\mathbf{u} = \mathbf{F} \tag{35}$$

where $\mathbf{M}$ and $\mathbf{K}$ are the global mass and global stiffness matrices assembled by each element. $\mathbf{F}$ is the vector of global external force. These matrices can be constructed as follows:

$$\mathbf{M}_{ij} = \begin{bmatrix} \mathbf{M}_{ij}^{uu} & \mathbf{M}_{ij}^{ua} & \mathbf{M}_{ij}^{ub} \\ \mathbf{M}_{ij}^{au} & \mathbf{M}_{ij}^{aa} & \mathbf{M}_{ij}^{ab} \\ \mathbf{M}_{ij}^{bu} & \mathbf{M}_{ij}^{ba} & \mathbf{M}_{ij}^{bb} \end{bmatrix} \tag{36}$$

$$\mathbf{K}_{ij} = \begin{bmatrix} \mathbf{K}_{ij}^{uu} & \mathbf{K}_{ij}^{ua} & \mathbf{K}_{ij}^{ub} \\ \mathbf{K}_{ij}^{au} & \mathbf{K}_{ij}^{aa} & \mathbf{K}_{ij}^{ab} \\ \mathbf{K}_{ij}^{bu} & \mathbf{K}_{ij}^{ba} & \mathbf{K}_{ij}^{bb} \end{bmatrix} \tag{37}$$

$$\begin{aligned} \mathbf{u}_i &= \{\mathbf{u}_i^u, \mathbf{u}_i^a, \mathbf{u}_i^b\} \\ \ddot{\mathbf{u}}_i &= \{\ddot{\mathbf{u}}_i^u, \ddot{\mathbf{u}}_i^a, \ddot{\mathbf{u}}_i^b\} \\ \mathbf{F}_i &= \left\{\mathbf{F}_i^u, \mathbf{F}_i^a, \mathbf{F}_i^b\right\} \end{aligned} \tag{38}$$

where

$$\begin{aligned} \mathbf{M}_{ij}^{rs} &= \int_{\Omega^e} \rho(\tilde{\mathbf{N}}_i^r)^T \tilde{\mathbf{N}}_j^s d\Omega \quad (r,s = u,a,b) \\ \mathbf{K}_{ij}^{rs} &= \int_{\Omega^e} (\tilde{\mathbf{B}}_i^r)^T \mathbf{D} \tilde{\mathbf{B}}_j^s d\Omega \quad (r,s = u,a,b) \end{aligned} \tag{39}$$

$$\begin{aligned} \mathbf{F}_i^u &= \int_{\Omega^e} \tilde{\mathbf{N}}_i \bar{\mathbf{b}} d\Omega + \int_{\Gamma_t} \tilde{\mathbf{N}}_i \bar{\mathbf{t}} d\Gamma \\ \mathbf{F}_i^a &= \int_{\Omega^e} \tilde{\mathbf{N}}_i (H(\mathbf{x}) - H(\mathbf{x}_i)) \bar{\mathbf{b}} d\Omega + \int_{\Gamma_t} \tilde{\mathbf{N}}_i (H(\mathbf{x}) - H(\mathbf{x}_i)) \bar{\mathbf{t}} d\Gamma \\ \mathbf{F}_i^b &= \int_{\Omega^e} \tilde{\mathbf{N}}_i (F_\alpha(\mathbf{x}) - F_\alpha(\mathbf{x}_i)) \bar{\mathbf{b}} d\Omega + \int_{\Gamma_t} \tilde{\mathbf{N}}_i (F_\alpha(\mathbf{x}) - F_\alpha(\mathbf{x}_i)) \bar{\mathbf{t}} d\Gamma \quad (\alpha = 1,2,3,4) \end{aligned} \tag{40}$$

In these equations, $\tilde{\mathbf{N}}_i$ and $\tilde{\mathbf{B}}_i^u$ are the shape functions and displacement gradient matrices of the XCQ4 algorithm for standard nodes, and the terms $\tilde{\mathbf{B}}_i^a$ and $\tilde{\mathbf{B}}_i^b$ are gradient matrices for enriched nodes given by

$$\begin{aligned} \tilde{\mathbf{B}}_i^u &= \begin{bmatrix} \tilde{N}_{i,x} & 0 \\ 0 & \tilde{N}_{i,y} \\ \tilde{N}_{i,y} & \tilde{N}_{i,x} \end{bmatrix} \\ \tilde{\mathbf{B}}_i^a &= \begin{bmatrix} (\tilde{N}_i(H(\mathbf{x}) - H(\mathbf{x}_i)))_{,x} & 0 \\ 0 & (\tilde{N}_i(H(\mathbf{x}) - H(\mathbf{x}_i)))_{,y} \\ (\tilde{N}_i(H(\mathbf{x}) - H(\mathbf{x}_i)))_{,y} & (\tilde{N}_i(H(\mathbf{x}) - H(\mathbf{x}_i)))_{,x} \end{bmatrix} \\ \tilde{\mathbf{B}}_i^b &= \begin{bmatrix} (\tilde{N}_i(F_\alpha(\mathbf{x}) - F_\alpha(\mathbf{x}_i)))_{,x} & 0 \\ 0 & (\tilde{N}_i(F_\alpha(\mathbf{x}) - F_\alpha(\mathbf{x}_i)))_{,y} \\ (\tilde{N}_i(F_\alpha(\mathbf{x}) - F_\alpha(\mathbf{x}_i)))_{,y} & (\tilde{N}_i(F_\alpha(\mathbf{x}) - F_\alpha(\mathbf{x}_i)))_{,x} \end{bmatrix} \quad (\alpha = 1,2,3,4) \end{aligned} \tag{41}$$

In this work, the general Newmark integration is adopted for time integration. Which has been widely employed for transient dynamic crack analyses. Under the assumption of linear acceleration at each time step and zero viscous damping, the acceleration form can be gained as follows [26,27]:

$$(\mathbf{M} + \beta\Delta t^2 \mathbf{K})\ddot{\mathbf{u}}_{t+\Delta t} = \mathbf{F}_{t+\Delta t} - \mathbf{K}(\mathbf{u}_t + \Delta t\dot{\mathbf{u}}_t + \Delta t^2(0.5 - \beta)\ddot{\mathbf{u}}_t) \tag{42}$$

where $\mathbf{F}_{t+\Delta t}$ is the vector of global external force, $t$ and $t + \Delta t$ are the last step and the present step, respectively and $\Delta t$ is the time step. If the value of $\ddot{\mathbf{u}}_{t+\Delta t}$ is known, $\mathbf{u}_{t+\Delta t}$ and $\dot{\mathbf{u}}_{t+\Delta t}$ can be evaluated by following equations:

$$\mathbf{u}_{t+\Delta t} = \mathbf{u}_t + \Delta t\dot{\mathbf{u}}_t + \Delta t^2(0.5 - \beta)\ddot{\mathbf{u}}_t + \beta\Delta t^2 \ddot{\mathbf{u}}_{t+\Delta t} \tag{43}$$

$$\dot{\mathbf{u}}_{t+\Delta t} = \dot{\mathbf{u}}_t + (1 - \gamma)\Delta t\ddot{\mathbf{u}}_t + \gamma\Delta t\ddot{\mathbf{u}}_{t+\Delta t} \tag{44}$$

where $\gamma$ and $\beta$ are the two constants that should guarantee the stability of the Newmark approach with the requirement of $\alpha \geqslant 0.5, \beta \geqslant 0.25(\alpha + 0.5)^2$ [13,34,38]. Therefore, $\gamma$ and $\beta$ are set to be 0.5 and 0.25 to make the method implicit and unconditionally stable with the second order accuracy.

## 6. Numerical results of DSIFs and discussions

In this section, with the purpose of investigating XCQ4 performance on the calculation of dynamic fracture behavior in isotropic and anisotropic solids, some representative numerical examples with simple and complicated configurations are analyzed. The DSIFs are calculated for different loading conditions and the selected cases only consider stationary crack. The obtained numerical results of all cases are compared with reference solutions from experimental or other numerical methods to validate the accuracy of the XCQ4 approach.

Two specific types of loading conditions: *type I* : *Step loading* and *type II* : *Sine loading* as shown in Fig. 7 are considered.

### 6.1. Edge cracked isotropic semi-infinite plate

In the context of homogenous property, the accuracy of DSIFs calculation by this method is confirmed for the edge cracked plate with geometric parameters as $H = 300$ mm, $W = 200$ mm, $d = 150$ mm and $a = 50$ mm. The imposed velocity $v$ is set to be 6.5 m/s and arises on the upper half of left edge as shown in Fig. 8. For other boundary, traction is free in this numerical example. The steel material is chosen with properties of the Young's modulus $E = 200$ GPa, the mass density $\rho = 7850$ kg/m$^3$ and the Poisson's ratio $\upsilon = 0.25$. Also, a plain strain condition is prescribed. The same problem was solved by Song et al. [34] using the displacement correlation technique (DCT) and Lee et al. [41] using linear superposition of stress wave solutions. Both related numerical solutions are taken as the reference solutions to verify the accuracy of the proposed method. The total mesh is 2417 elements including regular and irregular elements as shown in Fig. 8. The time step

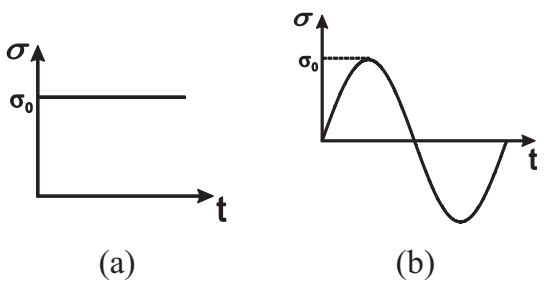


**Fig. 7.** (a) Step loading; (b) Sine loading.

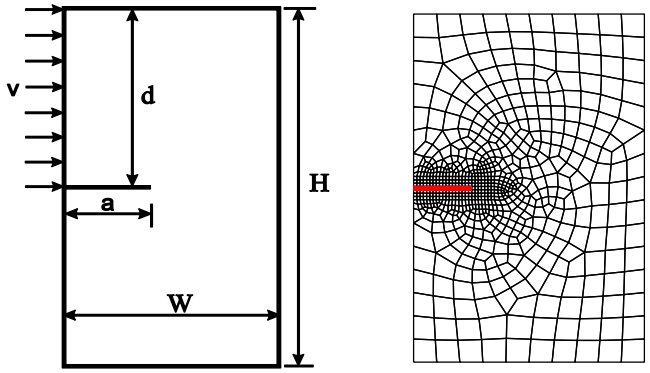


**Fig. 8.** Geometry of the edge cracked plate problem.

$\Delta t = 0.4 \times 10^6$ s is taken into account in the average acceleration method. The longitudinal wave speed $C_d$ can be obtained based on the basis material properties as follows:

$$C_d = \sqrt{\frac{E(1-\upsilon)}{\rho(1+\upsilon)(1-2\upsilon)}} = 5529.3 \text{ m/s} \tag{45}$$

The obtained numerical results are compared with the analytical solutions reported by Lee et al. [41] and reference solution given by Song et al. [34] in terms of DCT method as shown in Fig. 9. The horizontal axis denotes the value of normalized time $C_d t/a$. The ordinate axis signifies the normalized DSIFs by $E\upsilon\sqrt{a/\pi}/(2C_d(1-\upsilon^2))$. The time history of DSIFs is shown for the time from the initial loading to the first arrival of the scattered wave at the crack tip. The negative and positive values of $K_I$ and $K_{II}$ are induced, respectively when the stress waves generated by the imposed velocity reach the crack tip. It is clearly observed that the present numerical solution are in good agreement with reference solutions in the entire range of the considered time history.

The effect of mesh density on the accuracy of obtained numerical DSIFs is investigated for the same numerical example. Three discretization sizes are used as $25 \times 7$, $43 \times 13$ and $61 \times 19$. The comparison among the normalized DSIFs for three mesh arrangements as well as the analytical solution is depicted in Fig. 10. The present results indicate that the coarse mesh will induce the deviation from the analytical solution at earlier initial time and relatively apparent oscillations occur throughout the whole duration.

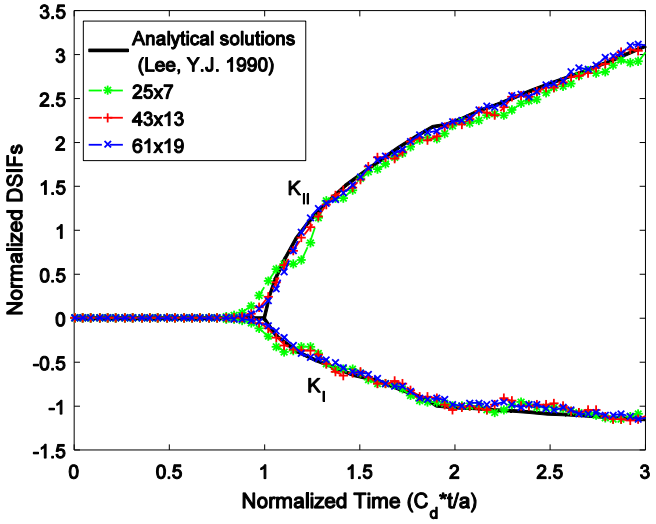


**Fig. 10.** Effect of mesh density on normalized DSIFs history.

Whereas better coincidence is obtained between the analytical solution and numerical results obtained by finer mesh. It is concluded that the mesh size has some effects on the accuracy of DSIFs and an appropriate mesh arrangement is necessary.

In Fig. 11, the sensitivity analysis for time step is investigated. The obtained results show that the too small time interval causes a slight oscillation when elastic waves reach the crack tip. However, with the increase of the time step, the oscillation at the initial stage of the arising value with respect to the normalized DSIFs is reduced, and the curve derived from large time step gets closer to the analytical solution by comparison with the one of small time step. It should be remarked that the sensitivity of time history with respect to the normalized DSIFs is related to the time step and appropriate time step is significant for alleviating the oscillation of the results.

For the edge cracked semi-infinite plate, it is obvious that the DSIFs should not be affected by the vertical distance $d$ defined from top edge to crack face as shown in Fig. 8, which means if the distance $d$ switches the value while other conditions are fixed, the time histories of DSIFs under different $d$ values are identical with each other. Upon the basis, three examinations of $d = 3H/6$,

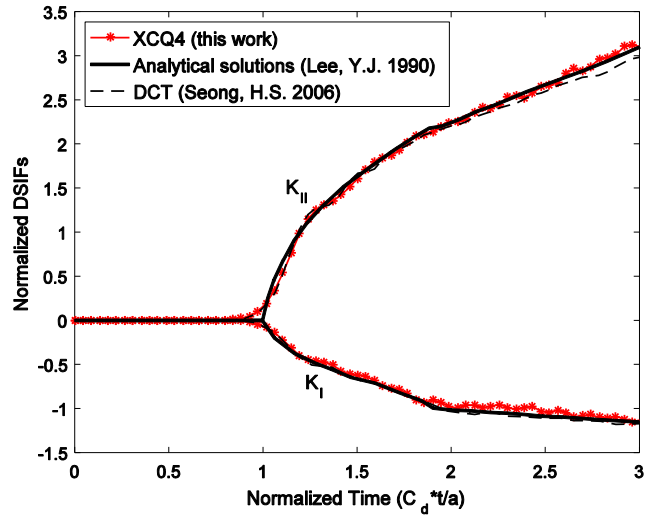


**Fig. 9.** Comparison of normalized DSIFs history with reference solutions.

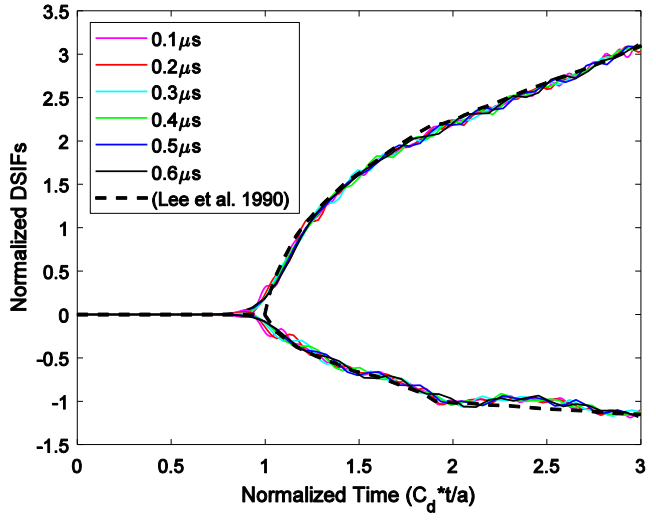


**Fig. 11.** Sensitivity analysis for time step with respect to the normalized DSIFs.

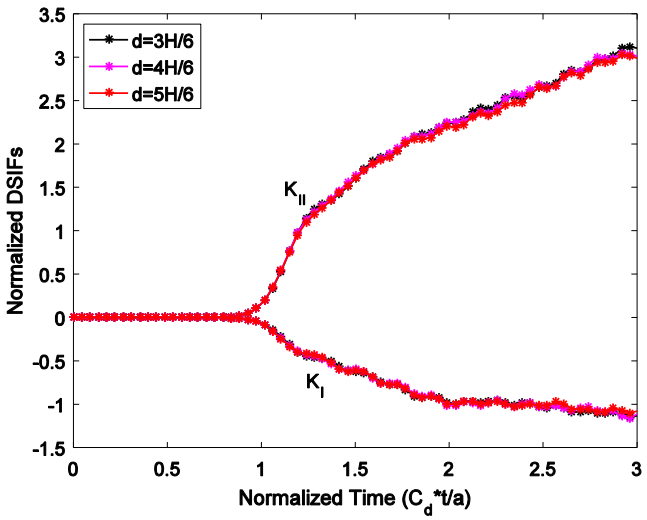


**Fig. 12.** Predicted time history of normalized DSIFs by XCQ4 under different d.

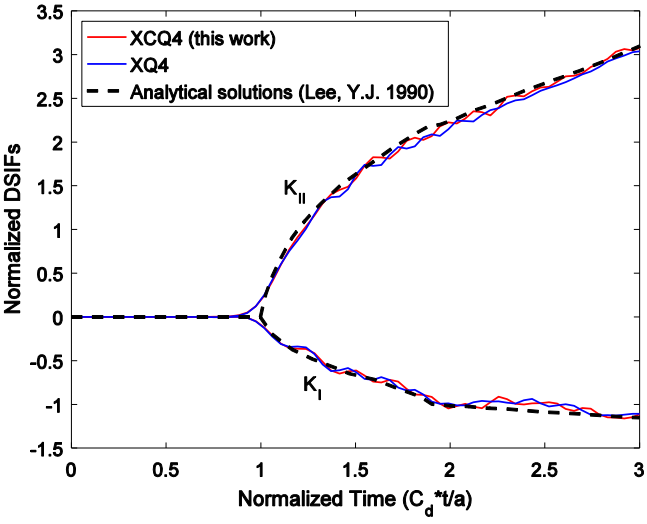


**Fig. 13.** Comparison of normalized DSIFs histories between XCQ4 and XQ4 method.

$d = 4H/6$ and $d = 5H/6$ are performed to investigate the stability of the developed method and their comparison is shown in Fig. 12. Since the wave reflection from the outer boundary needs much more time to reach the crack front, results obtained from different crack locations are close to each other, which has proven the reliable application of the XCQ4 for capturing the transient dynamic response in isotropic solid. Fig. 13 shows the comparison of numerical results derived from the XCQ4 and standard XQ4 method, it is obvious that curve obtained by the XCQ4 yields much better and closer to the analytical solution than that of the XQ4.

### *6.2. Center crack tension (CCT) specimen for both isotropic & orthotropic materials*

Let us consider a center cracked rectangular plate with dimension of $H = 40$ mm, $W = 20$ mm. A total of $50 \times 100$ structured elements as shown in Fig. 14 are used for the analysis. A crack length of $a = 4.8$ mm and a plain strain condition are considered. The instantaneous tension load $\sigma_0$ is applied to both top and bottom edges as shown in Fig. 7(a) and Fig. 14. The isotropic material parameters for this analysis are: the Young's modulus

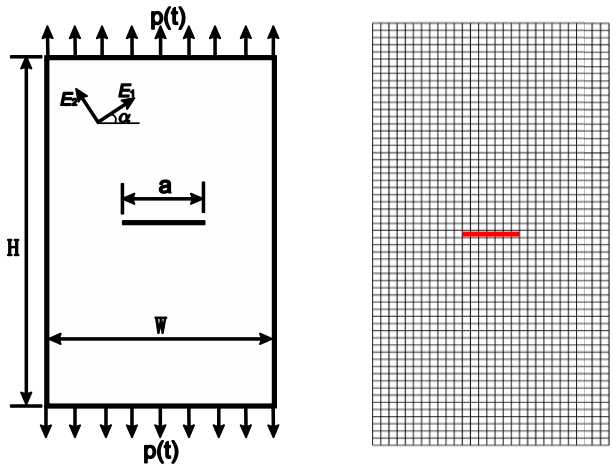


**Fig. 14.** Configuration of the plate with a central crack.

$E = 199.992$ GPa, the mass density $\rho = 5000\ \mathrm{kg/m^3}$ and the Poisson's ratio $\upsilon = 0.3$. The corresponding longitudinal wave speed can be calculated by $C_d = 7340$ m/s by Eq. (45). The numerical simulation is conducted by setting the time step $\Delta t = 0.05 \times 10^6$ s.

In Fig. 15, the obtained DSIF $K_I$ is compared with the reference solution of FEM [34] and the results computed by standard XQ4 method. The horizontal axis is the normalized time with respect to longitudinal wave speed $C_d$ and the vertical axis is normalized by $\sigma_0(\sqrt{\pi a/2})$. It is evident that the time variations of the normalized DSIFs calculated by XCQ4 are consistent with the reference solution and are much closer to reference solution compared with curves given by XQ4 method. It should be noted that, unlike the present XCQ4 approach, the mesh refinement in the vicinity of crack tip is necessary for the FEM as implemented by [34]. With respect to the physical meaning of the results, it can be explained that the incident longitudinal wave travelling to the crack tip from bar ends causes the value of normalized DSIF $K_I$ rising from 0 around $2C_d t/H = 1$. Then the Rayleigh wave generated by the initial incident waves propagates between two crack tips and the scattered longitudinal wave spreads from a crack tip to the closest boundary surface of the bar and the length of the bar. Finally the reflected wave from boundary side reaches the crack tip again

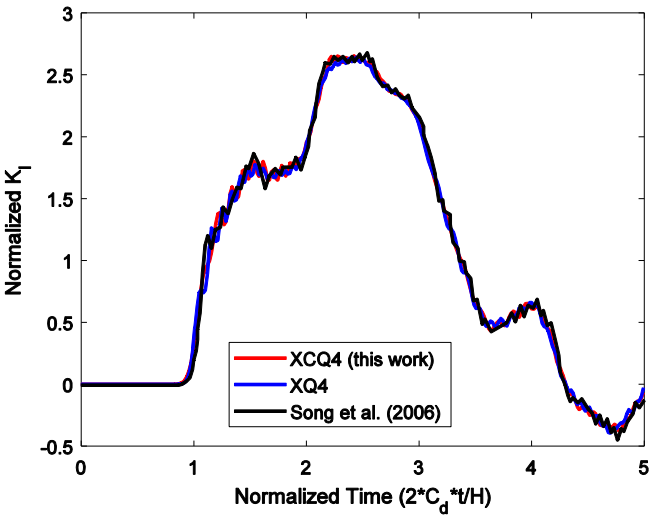


**Fig. 15.** Comparison between predicted time history of normalized mode I DSIF by XCQ4 and reference solution in isotropic solid.

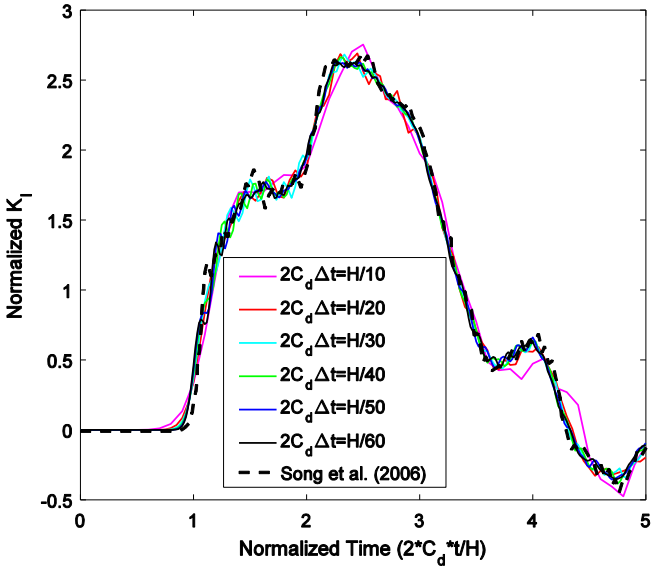


**Fig. 16.** Comparison of predicted mode I normalized DSIF history in different time steps in isotropic solid.

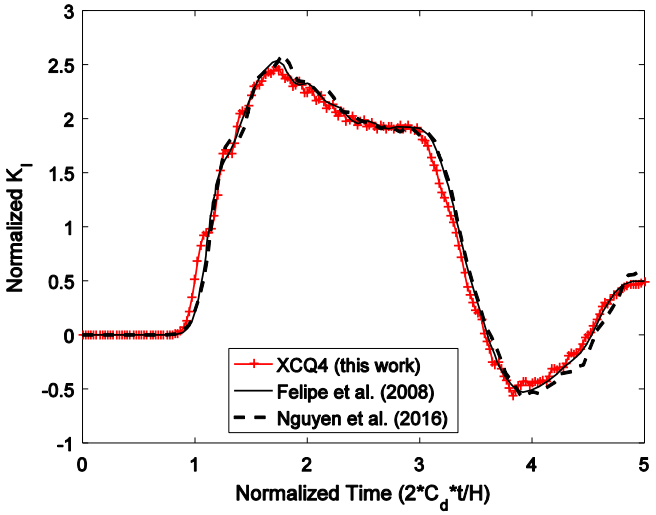


**Fig. 17.** Comparison between predicted mode I normalized DSIF history calculated by XCQ4 and reference solution in orthotropic solid.

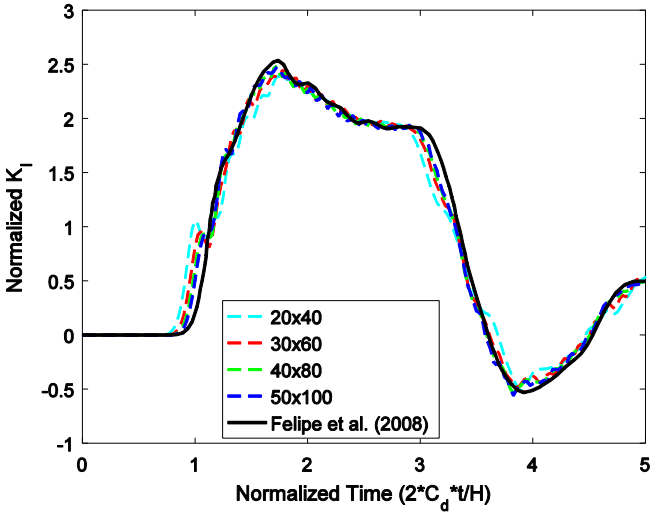


**Fig. 18.** Effect evaluation of mesh density on mode I normalized DSIF history calculated by XCQ4 in orthotropic solid.

and influences the value of normalized DSIF $K_I$ repeatedly. Since the contact condition at crack faces are not considered in this work, the negative value of normalized DSIF $K_I$ can be found.

To explore the sensitivity of the developed method to time intervals, the DSIF $K_I$ is calculated for various time increments from $2C_d\Delta t = H/10$ to $2C_d\Delta t = H/60$, which are shown in Fig. 16. The numerical results show that the larger time step is given the earlier initial rising time is observed, and the fluctuations in response become larger as well. In general, the DSIFs are in good agreement with reference solution for all cases under consideration, which confirms the accuracy and applicability of the XCQ4 to transient dynamic fracture in CCT isotropic specimens.

Next, the performance of XCQ4 for solving transient dynamic fracture problem in orthotropic material is investigated using the same CCT specimen. For this case, a plane stress condition is considered and the composite material properties are prescribed as: $E_1 = 118.30$ GPa, $E_2 = 54.80$ GPa, $G_{12} = 8.79$ GPa, $\upsilon_{12} = 0.083$, and $\rho = 1900$ kg/m$^3$. The time step $\Delta t = H/(80C_L)$ is taken into account and the same normalized coordinate axis as in the isotropic case is adopted. The wave speed along the $E_2$ material axis is defined as $C_L = \sqrt{C_{22}/\rho}$. Two reference solutions given by Felipe et al. [9] using a boundary element method and Nguyen et al. [10] employing X-RPIM are selected as our references, which are used to validate the accuracy of our XCQ4 method. As can be seen in Fig. 17, similar behaviors are obtained for these numerical methods, which certifies the feasibility of XCQ4 method in modelling dynamic fracture behaviors of orthotropic composites.

For center cracked orthotropic plate, the effect of mesh density on the time variation of DSIFs is investigated. Four patterns of mesh discretization, i.e., $20 \times 40$, $30 \times 60$, $40 \times 80$ and $50 \times 100$ are considered. Fig. 18 shows that the present results of DSIFs match well reference solution with increasing mesh density. Not surprisingly, there is a slight difference at the initial time and peak value of the dynamic response when the coarse mesh is taken.

In orthotropic composites, the orientation of the orthotropy has a significant impact on the fracture behavior, especially under dynamic loading condition. Here, we assess the completely anisotropic material characteristics in a plane stress condition by determining the degree of the material anisotropy through the matrix transformation of the elastic constants. The inclination angle of material $\alpha$ between the principle axis of material 1 and crack orientation is equal to 0°, 15°, 30°, 45° and 60°, respectively. The normalized results of DSIFs $K_I$ and $K_{II}$ obtained by XCQ4 are shown in Figs. 19 and 20, respectively. The available reference solutions by Felipe et al. [9] and Nguyen et al. [10] are taken for our comparison purpose. Consequently, similar dynamic responses for both failure modes are obtained. As a result, it can be concluded that the developed XCQ4 offers acceptable solutions of transient dynamic fracture response of anisotropic material.

### 6.3. Edge cracked plate with complicated shape

The purpose of this example is to demonstrate the applicability of XCQ4 to extract the DSIFs of anisotropic material with complex configuration. The geometry of the model and discretization are schematically depicted in Fig. 21. The related parameters are prescribed as: $H = 60$ mm, $L = 70$ mm, $S = 20$ mm, $D = 35$ mm, $d = 30$ mm, $w = 20$ mm. As shown in Fig. 7, either of two types of dynamic loadings is partially imposed on the right hand of the top edge; $typeI: \sigma_t = \sigma_0 \mathrm{H}(t)$ and $typeII: \sigma(t) = \sigma_0 \sin(\omega t)$ with $\omega = 2\pi/(50 \times 10^6)$, $\sigma_0 = 7.5 \times 10^6$ Pa. The boundary constraints

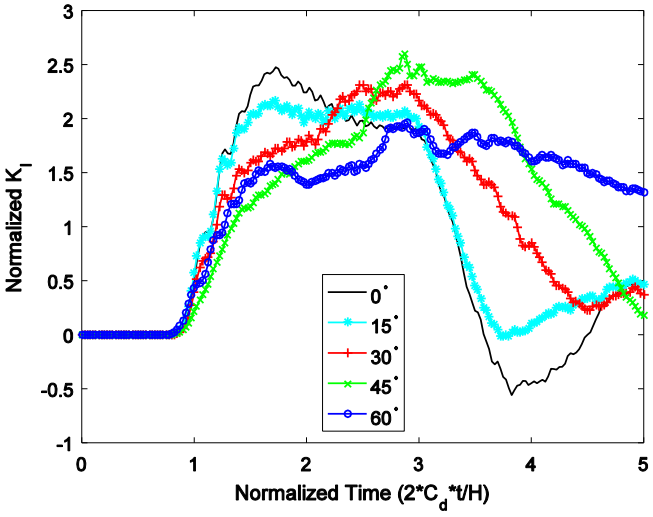


**Fig. 19.** Normalized mode I DSIF history for anisotropic case.

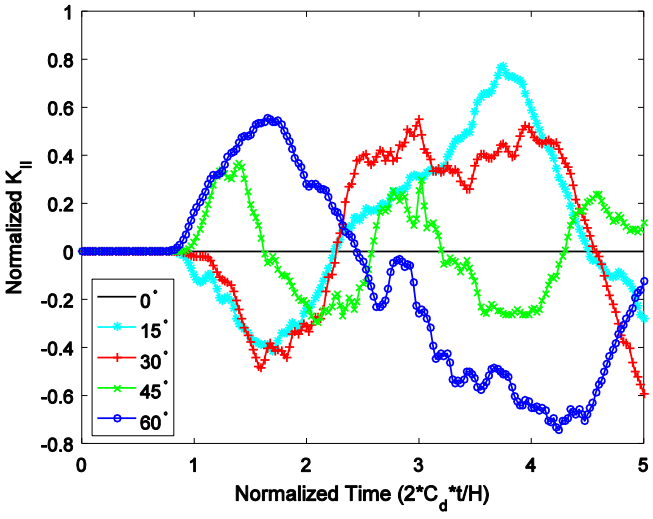


**Fig. 20.** Normalized mode II DSIF history for anisotropic case.

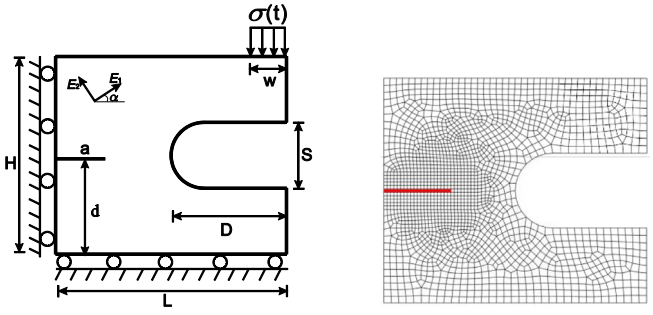


**Fig. 21.** Sophisticated geometry and discretization of edge cracked specimen.

in $x$-direction are set for all nodes on the left edge. Similarly, the nodes of bottom edge are restricted in $y$-direction. The initial crack length is given by $a = 18$ mm and the discretization of the domain is adopted as 1934 regular and irregular elements.

### 6.3.1. Isotropic material

The isotropic material properties are adopted as: the Young's modulus $E = 2.1 \times 10^{11}$ Pa, the mass density $\rho = 7800$ kg/m$^3$ and

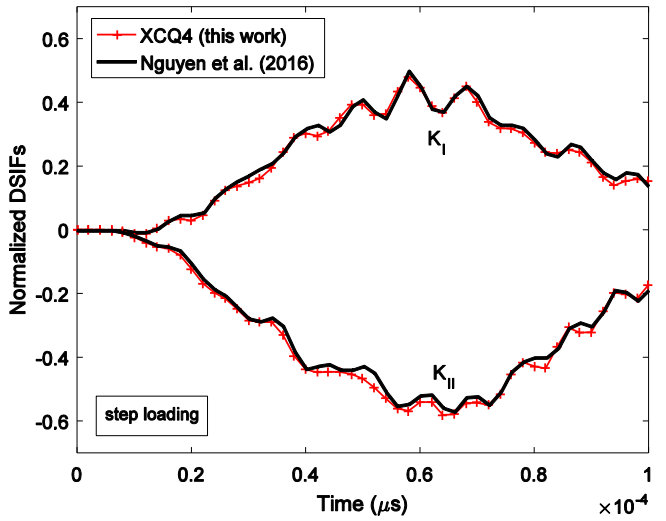


**Fig. 22.** Comparison of the normalized DSIFs by XCQ4 and reference solution under step loading condition in isotropic material.

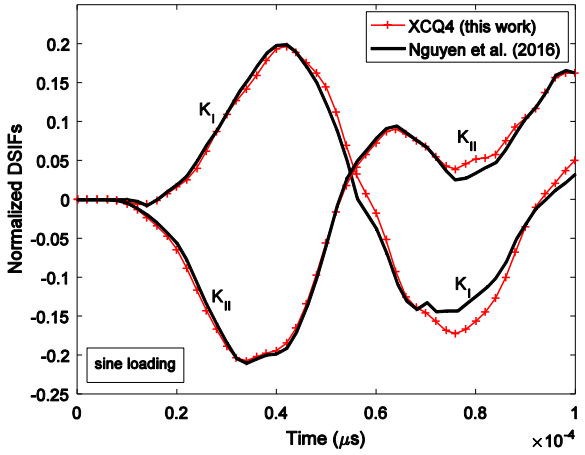


**Fig. 23.** Comparison of the normalized DSIFs by XCQ4 and reference solution under sine loading condition in isotropic material.

the Poisson's ratio $\upsilon = 0.285$. The same problem has been resolved numerically by Nguyen et al. [10] using the extended meshfree radial point interpolation method (X-RPIM). The corresponding results are used as the reference to verify the capability and performance of the proposed XCQ4 method.

The dynamic fracture behavior calculated by XCQ4 under two types of loading condition are collected and represented in Figs. 22 and 23, in which the normalized DSIFs with respect to $\sigma_0(\sqrt{\pi a})$ and time histories are given. Compared with original solution by Nguyen et al. [10] using X-RPIM, a good agreement between two solutions is obtained. We can also find out that the results under sine loading condition present smooth dynamic behavior, whereas the obvious oscillation can be observed in those under step loading.

### 6.3.2. Anisotropic material

Next, orthotropic material parameters are chosen the same as in the second example studied above. Again, the plane stress condition is assumed. The orthotropic material property is assigned to this structure and the corresponding dynamic fracture behavior is probed with variation of orthotropic angles such as 0°, 15°,

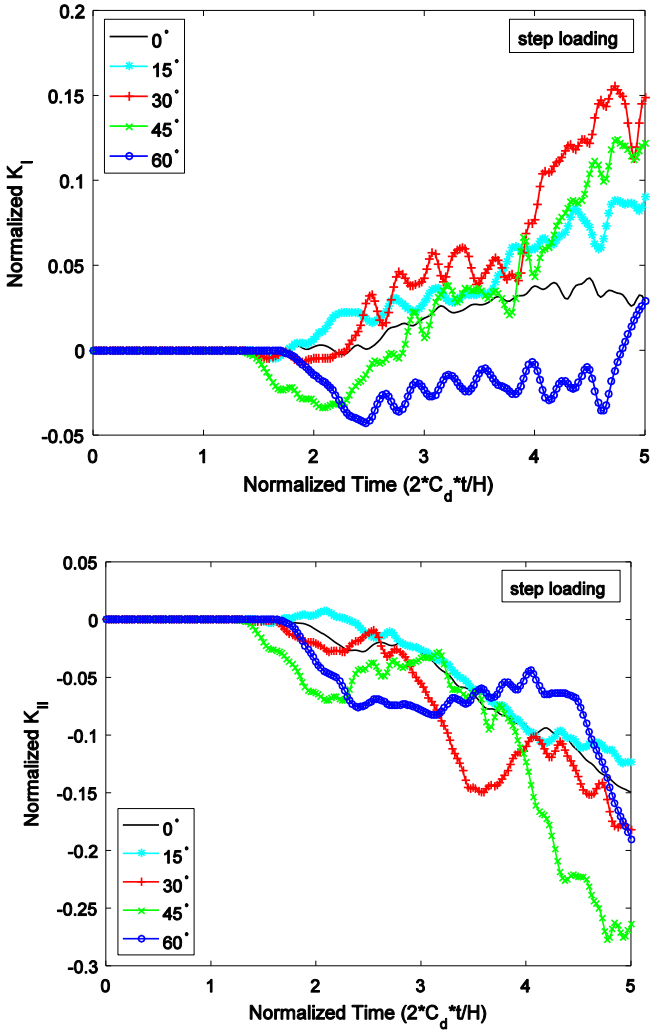


**Fig. 24.** The predicted normalized DSIFs history for anisotropic case under step loading.

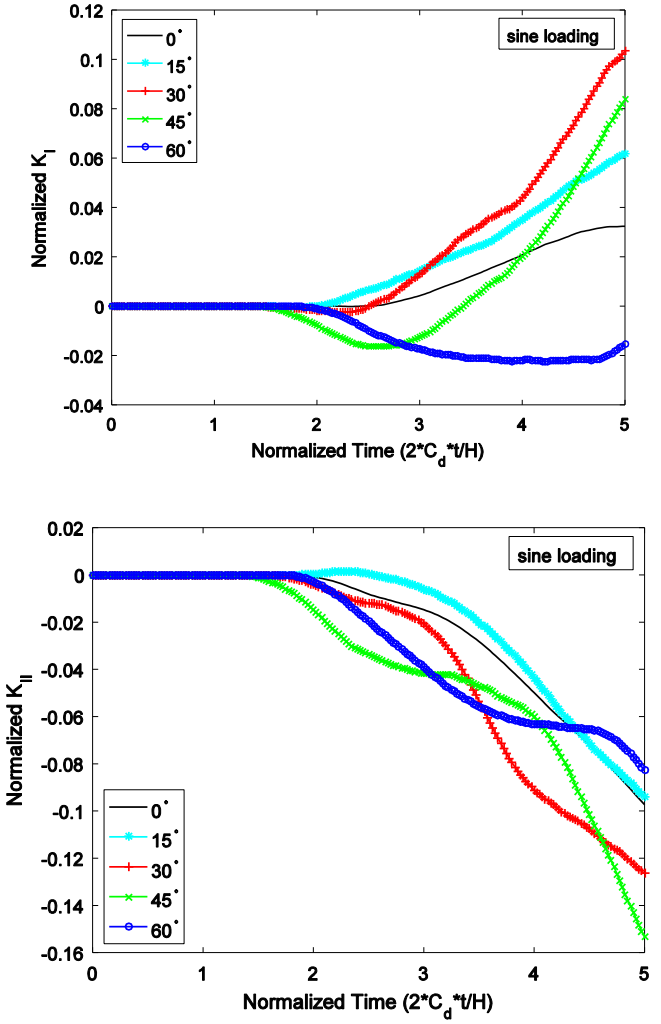


**Fig. 25.** The predicted normalized DSIFs history for anisotropic case under sine loading.

30°, 45° and 60°. Fig. 24 shows time variations of DSIFs $K_I$ and $K_{II}$ normalized by $\sigma_0(\sqrt{\pi a})$ under a step loading. The earlier initial time can be found in the case of inclination material angle $\alpha$ equal to 45° for both failure modes of DSIFs. In a similar manner, the relationship between two variables evaluated under sine loading condition is shown in Fig. 25. A similar behavior of transient dynamic fracture is obtained, and no evident oscillation exists. Due to the stiffness of material property in each direction differs apparently, the value of normalized DSIFs with respect to each case behaves differently. Moreover, the wave speed in domain significantly depends on the material property, so the curves in Figs. 24 and 25 deviate from the zero line at different normalized time as each case takes a different amount of time that longitudinal wave generated by the initial incident waves traveling to crack tip requires. In addition, it is interesting that the values of normalized DSIFs augment with the increase of $\alpha$ at initial stage whereas after $\alpha = 30°$, the corresponding values of DSIFs decline in Figs. 24 and 25. The peak value of the normalized mode-I and mdoe II DSIFs in this anisotropic case is decided by $\alpha = 30°$ and $\alpha = 45°$, respectively.

To reveal the effect of crack length on the characteristics of dynamic fracture in orthotropic material, we provide visualization on the correlation of normalized DSIFs and time history, provided that the principle axis of material 1 is perpendicular to the normal of crack orientation. Five values of the crack length $a = 9, 14, 18, 21$ mm are considered in this investigation. Based on the numerical results depicted in Fig. 26, the initial time of each case shows almost similar. However, it is interesting to see that the normalized values of both failure modes arise with decreasing the crack length. The oscillation problem that occurs more frequently in step loading condition than in sine loading one may be due to the propagation and reflection of the elastic stress waves in solids [10].

### 6.4. Plate with a central hole and two cracks

The last example is a plate with geometry size of height $H = 60$ mm and width $W = 30$ mm. One central hole with radius $r = 3.75$ mm and two cracks located at each horizontal side of the hole are set as shown in Fig. 27. The distance between two crack tips is $2a = 15$ mm. A step loading introduced in Fig. 7(a) and plane stress condition is assumed. The plate is discretized into 1842 elements as illustrated in Fig. 27.

Two types of material with respect to $\alpha = 0°$ are taken, and dynamic fracture response of this case is computed and analyzed. The quasi-isotropic material parameters are first considered as follows: the Young's modulus $E_1 = 220$ GPa, $E_2 = 219$ GPa, the shear modulus $G_{12} = 76.92$ GPa, the mass density $\rho = 5000$ kg/m$^3$ and the Poisson's ratio $\upsilon_{12} = 0.4286$. For orthotropic case, we only

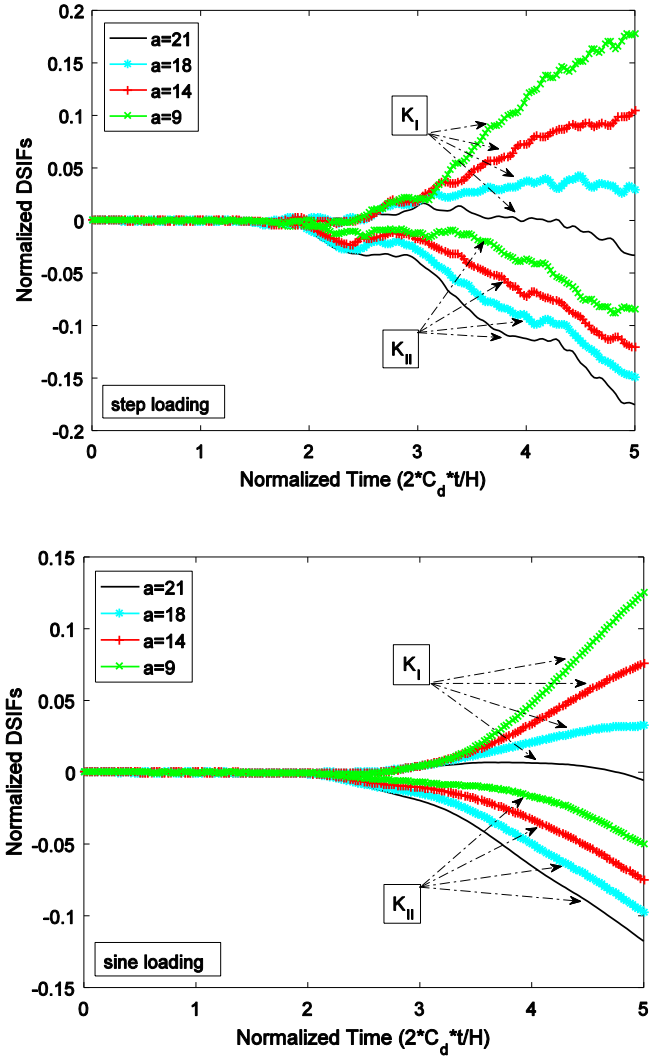


**Fig. 26.** The prediction for the influence of crack length on the normalized DSIFs history under different loading conditions.

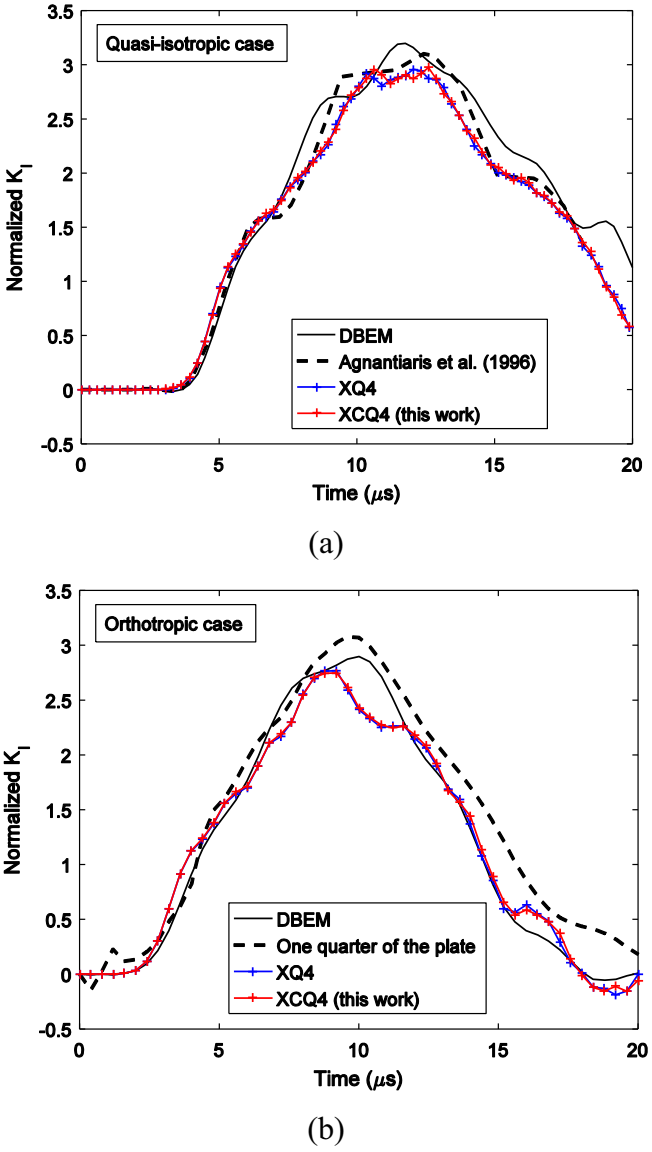


**Fig. 28.** The predicted normalized mode-I DSIF history for quasi-isotropic case (a) and orthotropic case (b) under step loading.

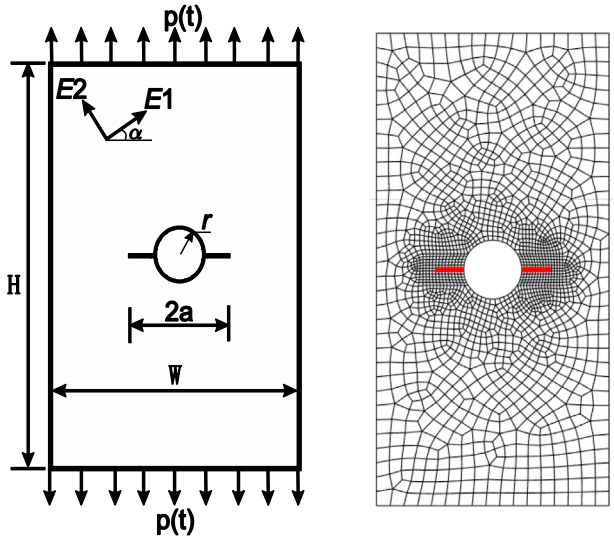


**Fig. 27.** Configuration of the plate with a central hole and two cracks.

change the longitudinal elastic moduli by $E_1 = 220$ GPa $E_2 = 440$ GPa and other material properties are taken the same to the quasi-isotropic case. The numerical simulations proceed with setting the time step $\Delta t = 0.28 \times 10^6$ s for quasi-isotropic material and $\Delta t = 0.4 \times 10^6$ s for the orthotropic material, and full integration scheme is required.

The numerical results reflecting the time history of normalized mode-I DSIF with respect to $\sigma_0(\sqrt{\pi a})$ are illustrated in Fig. 28. The reference solutions for quasi-isotropic case are given by Agnantiaris et al. [42] using the dual reciprocity principle, and Albuquerque et al. [43] by dual boundary element method (DBEM). For orthotropic case, Albuquerque et al. [43] offers the reference solution obtained by the discretization of one quarter of the plate via traction singular quarter point element. Both cases provide similar dynamic fracture response between numerical results by XCQ4 and the given references, although some slight deviation in regard of peak values can be found in each case. Due to the stiffer material property along longitudinal orientation in orthotropic material, the initial time of the dynamic fracture response is earlier than that of the quasi-isotropic case. The peak value of the

normalized mode-I DSIFs in quasi-isotropic case is larger than those in orthotropic one.

## 7. Conclusion

In this study, we have analyzed the dynamic fracture behaviors for both isotropic and anisotropic solids by our XCQ4. Some major desirable characteristics of the XCQ4 can be summarized as (1) remeshing procedure is no longer needed; (2) modelling of discontinuity is arbitrary without alignment to finite element mesh; (c) the stress recovery can be achieved; and (d) high accuracy for static and dynamic analysis. More information can be found in [25,37,39]. In this work, we have integrated the anisotropic enrichment functions for orthotropic composites into our XCQ4 formulation, which enables us to accurately capture the crack discontinuities and singularities in anisotropic materials. A series of numerical examples including isotropic and anisotropic materials have been considered and the obtained results of the DSIFs have been analyzed and discussed. Comparisons with reference solutions for DSIFs of single and mixed mode fracture problems have been made. High accuracy of the DSIFs for isotropic and anisotropic media is confirmed, revealing the accuracy and better performance of the XCQ4. The applicability of our XCQ4 to solve complex geometries in dynamic fracture under different loadings is also explored. The present approach offers acceptable solutions of DSIFs in all considered problems. Nevertheless, further studies on dynamic fracture for other complex materials such as multiphase composite materials, delamination in laminate composites, dynamic crack propagation under cyclic loading, etc. by the present XCQ4 would be very interesting.

## Acknowledgements

The financial supports of the Grant of Japan (No. 24-246078) and National CSC are gratefully acknowledged. The authors would like to thank all the reviewers for their valuable comments and suggestions.

## References

[1] Muskhelishvili NI. Some basic problems on the mathematical theory of elasticity. New York: Springer Science & Business Media; 1977.
[2] Kulikov GM, Plotnikova SV. Strong sampling surfaces formulation for laminated composite plates. Compos Struct 2017;172:73–82.
[3] Wu H, Fan GF, Huang M, Geng L, Cui XP, Chen RC, et al. Fracture behavior and strain evolution of laminated composites. Compos Struct 2017;163:123–8.
[4] Nobile L, Carloni C. Fracture analysis for orthotropic cracked plates. Compos Struct 2005;68:285–93.
[5] Covezzi F, Miranda SD, Marfia S, Sacco E. Complementary formulation of the TFA for the elasto-plastic analysis of composites. Compos Struct 2016;156:93–100.
[6] Arab SB, Rodrigues JD, Bouaziz S, Haddar M. A finite element based on equivalent single layer theory for rotating composite shafts dynamic analysis. Compos Struct 2017. http://dx.doi.org/10.1016/j.compstruct.2017.06.052.
[7] Tan A, Hirose S, Zhang Ch, Wang CY. A time-domain BEM for transient wave scattering analysis by a crack in anisotropic solids. Eng Anal Bound Elem 2005;29:610–23.
[8] Tan A, Hirose S, Zhang Ch. A time-domain collocationi-Galerkin BEM for transient dynamic crack analysis in anisotropic solids. Eng Anal Bound Elem 2005;29:1025–38.
[9] Felipe GS, Zhang Ch, Saez A. A two-dimensional time-domain boundary element method for dynamic crack problems in anisotropic solids. Eng Fract Mech 2008;75:1412–30.
[10] Nguyen NT, Bui TQ, Truong TT. Transient dynamic fracture analysis by an extended meshfree method with different crack-tip enrichments. Meccanica. 2017;52:2363–90.
[11] Nguyen NT, Bui TQ, Truong TT. Crack growth modeling in elastic solids by the extended meshfree Galerkin radial point interpolation method. Eng Ana Bound Elem 2014;44:87–97.
[12] Ghorashi SS, Mohammadi S, Sabbagh-Yazdi SR. Orthotropic enriched element free galerkin method for fracture analysis of composites. Eng Fract Mech 2011;78:1906–27.
[13] Liu P, Bui QT, Zhang Ch, Yu TT, Liu GR, Golub MV. The singular edge-based smoothed finite element method for stationary dynamic crack problems in 2D elastic solids. Comput Methods Appl Mech Eng 2012;233–236:68–80.
[14] Bui TQ, Hirose S, Zhang Ch, Rabczuk T, Wu CT, Saitoh T, Lei J. Extended isogeometric analysis for dynamic fracture in multiphase piezoelectric/piezomagnetic composites. Mech Mater 2016;97:135–63.
[15] Singh SK, Singh IV, Mishra BK, Bhardwaj G, Bui TQ. A simple, efficient and accurate Bézier extraction based T-spline XIGA for crack simulations. Theore Appl Fract Mech 2017;88:74–96.
[16] Caliri MF, Ferreira AJM, Tita V. A review on plate and shell theories for laminated and sandwich structures highlighting the finite element method. Compos Struct 2016;156:63–77.
[17] Bayesteh H, Mohammadi S. XFEM fracture analysis of shells: the effect of crack tip enrichments. Comput Mater Sci 2011;50:2793–813.
[18] Nasirmanesh A, Mohammadi S. XFEM buckling analysis of cracked composite plates. Compos Struct 2015;131:333–43.
[19] Nasirmanesh A, Mohammadi S. Eigenvalue buckling analysis of cracked functionally graded cylindrical shells in the framework of the extended finite element method. Compos Struct 2016;159:548–66.
[20] Unnikrishnan V, Reddy JN. Finite elements in analysis and design. Compos Struct 2012;49. 13-8.
[21] Shetty N, Shahabaz SM, Sharma SS, Shetty SD. A review on finite element method for machining of composite materials. Compos Struct 2017;176:790–802.
[22] Bui TQ, Zhang Ch. Extended finite element simulation of stationary dynamic cracks in piezoelectric solids under impact loading. Comput Mater Sci 2012;62:243–57.
[23] Bui QT, Zhang Ch. Analysis of generalized dynamic intensity factors of cracked magnetoelectroelastic solids by X-FEM. Finite Elem Anal Des 2013;69:19–36.
[24] Bui QT. Extended isogeometric dynamic and static fracture analysis for cracks in piezoelectric materials using NURBS. Comput Methods Appl Mech Eng 2015;295:470–509.
[25] Kang ZY, Bui QT, Saitoh T, Hirose S. Quasi-static crack propagation simulation by an enhanced nodal gradient finite element with different enrichments. Theor Appl Fract Mech 2017;87:61–77.
[26] Mohammadi S. Extended finite element method. United Kingdom: Wiley/Blackwell publishers; 2008.
[27] Mohammadi S. XFEM fracture analysis of composites. United Kingdom: Wiley; 2012.
[28] Asadpoure A, Mohammadi S, Vafai A. Crack analysis in orthotropic media using the extended finite element method. Thin Wall Struct 2006;44:1031–8.
[29] Asadpoure A, Mohammadi S. Developing new enrichment functions for crack simulation in orthotropic media by the extended finite element method. Int J Numer Methods Eng 2007;69:2150–72.
[30] Hattori G, Rojas R, Saez A, Sukumar N. New anisotropic crack-tip enrichment functions for the extended finite element method. Comput Mecc 2012;50:591–601.
[31] Motamedi D, Mohammadi S. Dynamic analysis of fixed cracks in composites by the extended finite element method. Eng Fract Mech 2010;77:3373–93.
[32] Motamedi D, Mohammadi S. Dynamic crack propagation analysis of orthotropic media by the extended finite element method. Int J Fract 2010;161:21–39.
[33] Motamedi D, Mohammadi S. Fracture analysis of composites by time independent moving-crack orthotropic XFEM. Int J Mech Sci 2012;54:20–37.
[34] Song SH, Paulino GH. Dynamic stress intensity factors for homogeneous and smoothly heterogeneous materials using the interaction integral method. Int J Solids Struct 2006;43:4830–66.
[35] Albuquerque EL, Sollero P, Aliabadi MH. Dual boundary element method for anisotropic dynamic fracture mechanics. Int J Numer Methods Eng 2004;59:1187–205.
[36] Rubio-Gonzalez C, Manzon JJ. Response of finite cracks in orthotropic materials due to concentrated impact shear load. J Appl Mech (ASME). 1999;66:485–91.
[37] Bui QT, Vo DQ, Zhang Ch, Nguyen DD. A consecutive-interpolation quadrilateral element (CQ4): formulation and applications. Finite Elem Anal Des 2014;84:14–31.
[38] Bui QT, Nguyen DD, Zhang XD, Hirose S, Batra RC. Analysis of 2-dimensional transient problems for linear elastic and piezoelectric structures using the consecutive-interpolation quadrilateral element (CQ4). Eur J Mech A/Solids 2016;58:112–30.
[39] Kang ZY, Bui QT, Nguyen DD, Saitoh T, Hirose S. An extended consecutive-interpolation quadrilateral element (XCQ4) applied to linear elastic fracture mechanics. Acta Mech 2015;226:3991–4015.
[40] Sharma K, Bui QT, Zhang Ch, Bhargava RR. Analysis of a subinterface crack in piezoelectric biomaterials with the extended finite element method. Eng Fract Mech 2013;104:114–39.
[41] Lee YJ, Freund LB. Fracture initiation due to asymmetric impact loading of an edge cracked plate. ASME J Appl Mech 1990;57:104–11.
[42] Agnantiaris JP, Polyzos D, Beskos DE. Some studies on dual reciprocity BEM for elastodynamics. Comput Mech 1996;17:270–7.
[43] Albuquerque EL, Sollero P, Aliabadi MH. Dual boundary element method for anisotropic dynamic fracture mechanics. Int J Numer Methods Eng 2004;59:1187–205.